Author Manuscript

Author Manuscript

Author Manuscript

Author Manuscript

HHS Public Access

Author manuscript

Ophthalmic Genet. Author manuscript; available in PMC 2022 June 01.

Published in final edited form as:

Ophthalmic Genet. 2021 June ; 42(3): 252–265. doi:10.1080/13816810.2021.1888132.

Bardet-Biedl syndrome-7 (*BBS7*) shows treatment potential and a cone-rod dystrophy phenotype that recapitulates the non-human primate model

Tomas S. Aleman[a,b,c], **Erin C. O'Neil**[a,b,c], **Keli O'Connor**[a,b], **Yu You Jiang**[a,b], **Isabella A. Aleman**[a,b], **Jean Bennett**[a,b], **Jessica I. W. Morgan**[a,b], **Brian W. Toussaint**[d,e]

[a]Scheie Eye Institute at the Perelman Center for Advanced Medicine, University of Pennsylvania, Philadelphia, Pennsylvania, USA

[b]Center for Advanced Retinal and Ocular Therapeutics, University of Pennsylvania, Philadelphia, Pennsylvania, USA

[c]Division of Ophthalmology of the Children's Hospital of Philadelphia, Department of Ophthalmology, University of Pennsylvania, Philadelphia, Pennsylvania, USA

[d]Christiana Care Health System, Wilmington, Delaware, USA

[e]Department of Ophthalmology, Lewis Katz School of Medicine, Temple University, Philadelphia, Pennsylvania, USA

Abstract

Purpose: To provide a detailed ophthalmic phenotype of two male patients with Bardet-Biedl Syndrome (BBS) due to mutations in the *BBS7* gene

Methods: Two brothers ages 26 (Patient 1, P1) and 23 (P2) underwent comprehensive ophthalmic evaluations over three years. Visual function was assessed with full-field electroretinograms (ffERGs), kinetic and chromatic perimetry, multimodal imaging with spectral domain optical coherence tomography (SD-OCT), fundus autofluorescence (FAF) with short- (SW) and near-infrared (NIR) excitation lights and adaptive optics scanning light ophthalmoscopy (AOSLO).

Results: Both siblings had a history of obesity and postaxial polydactyly; P2 had diagnoses of type 1 Diabetes Mellitus, Addison's disease, high-functioning autism-spectrum disorder and −12D myopia. Visual acuities were better than 20/30. Kinetic fields were moderately constricted. Cone-mediated ffERGs were undetectable, rod ERGs were ~80% of normal mean. Static perimetry showed severe central cone and rod dysfunction. Foveal to parafoveal hypoautofluorescence, most obvious on NIR-FAF, co-localized with outer segment shortening/loss and outer nuclear layer thinning by SD-OCT, and with reduced photoreceptors densities by AOSLO. A structural-

CONTACT Tomas S. Aleman aleman@pennmedicine.upenn.edu Perelman Center for Advanced Medicine, University of Pennsylvania, 3400 Civic Center Boulevard, Philadelphia, PA 19104, USA.

Declaration of interest

The authors report no conflicts of interest. The authors alone are responsible for the content and writing of this article.

Financial and competing interests

JIWM is an inventor on US Patent 8226236.

Author Manuscript Author Manuscript Author Manuscript Author Manuscript

functional dissociation was confirmed for cone- and rod-mediated parameters. Worsening of the above abnormalities was documented by SD-OCT and FAF in P2 at 3 years. Gene screening identified compound heterozygous mutations in *BBS7* (p.Val266Glu: c.797 T > A of maternal origin; c.1781_1783delCAT, paternal) in both patients.

Conclusions: *BBS7*-associated retinal degeneration may present as a progressive cone-rod dystrophy pattern, reminiscent of both the murine and non-human primate models of the disease. Predominantly central retinal abnormalities in both cone and rod photoreceptors showed a structural-functional dissociation, an ideal scenario for gene augmentation treatments.

Keywords

Bardet-Biedl; BBS; BBS7; OCT; cone dystrophy; cone-rod dystrophy; adaptive optics ophthalmoscopy; retinitis pigmentosa; RP

Introduction

Bardet-Biedl syndrome (BBS) describes an autosomal recessive, genetically heterogeneous condition, characterized by the presence of a photoreceptor degeneration variably associated with truncal obesity, postaxial polydactyly, hypogonadism, renal and cardiac abnormalities, and variable cognitive impairment (1–9). Prevalence estimates are variable and range from 1:18,000 to 1:160,000(5). Retinal degeneration is the most consistent feature(10). Indeed, BBS is one of the most common forms of syndromic retinitis pigmentosa (RP) (5,11). Although there is variability in disease severity, patients typically present with nyctalopia and visual field defects in the first decade of life, progressing to severe central vision loss and legal blindness at a relatively young age (5,12–14). At some point in the disease patients develop a pigmentary retinopathy indistinguishable from the classic appearance of RP, in the majority of the patients associated with a rod-greater-than-cone dystrophy (RCD) pattern of dysfunction, less frequently a cone-rod (CRD) dystrophy, rarely a cone dystrophy (COD) pattern (12–16).

Mutations in up to 22 genes have been identified to date, all encoding proteins expressed in primary cilia, including retinal photoreceptors (6,17,18). BBS is thus considered a ciliopathy, with genetic, mechanistic and phenotypic overlaps with other syndromic ciliopathies such as McKusick-Kaufmann, Alström, Meckel Gruber, Joubert, Senior-Løken, and Mainzer-Zaldino syndromes (6,11,17). The genetic heterogeneity and the role of modifying genes appears to explain the variable severity of the retinal phenotype as well as of the associated systemic abnormalities, even among family members who harbor identical mutations (4,5,14,19). Of the currently known disease-causing genes, eight (*BBS1, BBS2, BBS4, BBS5, BBS7, BBS8, BBS9,* and *BBS18*) encode proteins that play a role in assembly of a protein complex known as the BBSome, which plays a crucial role in protein trafficking (11,20–26). Other genes play a role in the assembly (*BBS6, BBS10*, and *BBS12*), or protein trafficking (*BBS3, BBS14*, and *BBS17*) within cilia (5,27,28). The precise function of other genes remains unknown but are thought to also be closely related to the BBSome. Specifically within the retina, abnormalities are thought to be related to structural and/or functional damage to the cilium connecting photoreceptor inner and outer segments, likely

Author Manuscript Author Manuscript Author Manuscript Author Manuscript

from accumulation of mislocalized proteins (26,29). By far, mutations in *BBS1* and *BBS10* explain most of the BBS cases.

BBS7 was identified as a disease-causing gene in 2003(4). Although *BBS7* mutations account for only 3–7% of the BBS cases, the encoded protein is part of the core of the BBSome complex (11,18,19,24,26,30). The few descriptions of the *BBS7* human retinal phenotype are limited and suggest a higher disease burden with a greater expression of cardinal features than patients with other gene mutations such as *BBS1* or *BBS8* (31–34). The paucity of descriptions of the BBS7 human phenotype contrasts with the availability of animals models of this specific form of BBS, including the recent description of a non-human primate (NHP) model (35). In this report we present a detailed phenotypic description of two patients with BBS7 and draw direct comparisons with the animal models in hopes the exercise will help us gain a better understanding not only of BBS7, but of the much larger group of syndromic retinal ciliopathies, including their treatment potential by gene therapy.

Methods

Two patients underwent a complete ophthalmic examination and testing as part of their standard of care, complemented by detailed retinal phenotyping over the course of 3 years as research. Informed consent was obtained; procedures adhered to the Declaration of Helsinki and were approved by the institutional review board (protocol #815348). Automated static perimetry was performed using a modified Humphrey Field Analyzer (HFA II–i, Carl Zeiss Meditec, Dublin, CA) using a 200-ms long, 1.7° diameter stimuli, presented at 2° intervals along a horizontal profile that extended to 30° of eccentricity. Light-adapted perimetry was performed with an achromatic stimulus on a white (10 $cd.m^{-2}$) background; two color dark-adapted perimetry was performed with 500 nm and 650 nm stimuli (36,37). Spectral sensitivity differences in the dark-adapted state were used to define photoreceptor mediation of the stimuli. The sensitivity profile corresponds to the retinal region scanned with spectral domain optical coherence tomography (SD-OCT; see below). A standard full-field electroretinogram (ffERG) was recorded using a computer-based system (Espion e3, Diagnosys LLC, Littleton, MA), following the recommendations of the standards of the International Society for Clinical Electrophysiology of Vision (ISCEV) (38,39). Rod-mediated responses were elicited with a dim white flash (0.01 $phot\text{-}cd.s.m^{-2}$). A white flash (3 $phot\text{-}cd.s.\ m^{-2}$) in the dark adapted state was used to evoke a combined rod-cone response and in light-adapted conditions in response to a 1 Hz or 30 Hz flicker to elicit cone-mediated ERGs.

SD-OCT, en-face near infrared (NIR) reflectance (REF) and fundus autofluorescence (FAF) imaging using NIR and short-wavelength (SW) excitation wavelengths was performed using a Spectralis-HRA system (Heidelberg Engineering GmbH, Heidelberg, Germany). Segmentation of the SD-OCT images was performed with the built-in segmentation software of the Spectralis system, supervised to ensure correct identification of the different laminar boundaries by examining the longitudinal reflectivity profiles (LRPs) with a publicly available software (http://imagej.nih.gov/ij/links.html)(37) (40).

Author Manuscript Author Manuscript Author Manuscript Author Manuscript

A custom adaptive optics scanning light ophthalmoscope (AOSLO) was also used in this study (41,42). Patients were aligned to the AOSLO using a dental impression. Wavefront sensing was done using an 848 nm superluminescent diode with a full-width at half-maximum bandwidth (FWHM) of 26 nm (Superlum, Ireland) and aberration correction was provided by a 97 actuator deformable mirror (Alpao SAS, France). Confocal and split-detection images were acquired at 17.85 frames per second over a 1° by 1° field of view using a superluminescent diode centered at 795 nm with FWHM of 15.3 nm (Superlum, Ireland) and a photomultiplier tube (PMT, Hamamatsu Corporation, Japan). The patient was instructed to fixate (using the imaged eye) at a target while the AOSLO image sequences were acquired along the temporal meridian. A custom strip-registration algorithm was used for intra-frame strip-based registration and dewarping of the AOSLO images (41,43,44). Reference frames for registration were chosen automatically from the image sequences and 50 frames were registered and averaged (45,46). Averaged images were then automatically montaged using a previously described algorithm (47). Regions of interest (ROI) were at the fovea and along the temporal meridian. Cones, rods, and RPE cells were identified within the ROIs in a semi-automated fashion, using a previously described algorithm, and densities were extracted from the cell locations (48,49).

Results

The proband in this study is a 26-year-old male patient (Patient 1, P1) referred for ophthalmic evaluation accompanied by his asymptomatic brother and mother. He had an ophthalmic history of moderate myopic astigmatism and two strabismus surgeries at ages 10 and 14. His medical history was significant for postaxial polydactyly of the right foot. He was obese (BMI = 50.2) but had no history of diabetes mellitus, kidney disease, or hypogonadism. There was no known parental consanguinity. Parents ancestry was German-Scottish on the maternal side, Irish-Welsh on the paternal side. There was no family history of retinal degeneration or blindness; an uncle, two aunts and grandfather on the maternal side are reportedly myopes. The patient reported blurred vision for the preceding 6 months associated with photophobia necessitating use of sunglasses and a hat. He reported no difficulty with driving at night or negotiating obstacles. He noted difficulty distinguishing dark blue colors. On initial evaluation, best corrected visual acuity was 20/30 in the right eye and 20/20 in the right eye (Spherical equivalent, SE, −0.50D) in each eye. He demonstrated a right intermittent exotropia. Color vision testing (Farnsworth, D15), intraocular pressures, and anterior segment examinations were normal. Fundus examination demonstrated a tilted optic nerves and parafoveal depigmentation as a subtle bull’s eye maculopathy (Figure 1a, P1). The fundus exam appearance did not change over the 3-year follow up period. SW-FAF imaging showed an incomplete parafoveal annulus of tenuous hypo-autofluorescence, more obvious in supero-nasal parafovea that surrounds a small ring of juxtafoveal hyper-autofluorescence (Figure 1a). By contrast, there was a complete parafoveal annulus of dense hypo-autofluorescence on NIR-FAF imaging that surrounds tightly a normal appearing foveal center (Figure 1a).

The patient’s 22-year-old only brother (P2) was asymptomatic. He had an ophthalmic history notable for high myopia in both eyes (SE −11.50). On questioning medical history was notable for similar postaxial polydactyly, Type 1 Diabetes Mellitus, Addison’s disease,

Author Manuscript Author Manuscript Author Manuscript Author Manuscript

obesity (BMI = 32.3), and high-functioning autism spectrum disorder. His best corrected visual acuity was 20/30 in each eye. Color vision testing revealed multiple errors with a tritan axis of confusion. Intraocular pressures were normal and anterior segment examination was unremarkable. Fundus examination revealed a myopic conus and a depigmented peripapillary and nasal fundus appearance with visualization of the choroidal vasculature (Figure 1a, P2). The normal SW-FAF signal is centered by a dark fovea resulting from pre-RPE screening by the macular pigment (MP) of the SW excitation lights used in this work; the normal NIR-FAF is characterized by a local maximum near the foveal center caused by greater content of melanin within taller central RPE cells (Figure 1a, *insets*) (50–52). SW-FAF in P2 demonstrated a darker than normal foveal center surrounded by a ring of juxtafoveal hyper-autofluorescence (Figure 1a, P2, *red arrow*). The local hyperautofluorescence exceeded the normal increase in SW-FAF signal in the juxtafovea caused by a local reduction in the MP optical density (MPOD) or 'shoulder' of the MPOD, illustrated in a representative normal subject shown (Figure 1a, *inset, red arrow*) (51,53–56). The central round hypoautofluorescent region had a similar appearance on NIR-FAF also surrounded by a juxtafoveal ring of mild NIR hyperautofluorescence (Figure 1a).

SD-OCT imaging was used to explore the underlying structural abnormalities in cross-section (Figure 1b). P1 showed obvious foveal and juxtafoveal thinning of the photoreceptor outer nuclear layer (ONL), including the photoreceptor axons. At the foveal center there is approximation of the inner segment ellipsoid band (EZ) to the apical retinal pigmented epithelium and Bruch's membrane (RPE/BrM) signals, likely from shortening and/or loss of photoreceptor outer segments (Figure 1b) (40,57–63). While the EZ and outer limiting membrane (OLM) are visible at the foveal center, the EZ becomes undiscernible in the juxtafoveal region (<0.75 mm of eccentricity), where the OLM abuts the apical RPE (Figure 1b, between yellow arrows) (64,65). This segment corresponds to the area of hypoautofluorescence on SW-FAF and NIR-FAF that is slightly eccentric toward the nasal side of the fovea (Figure 1a). With increasing eccentricity into the parafovea and pericentral retina, the retinal lamination regains a normal appearance with the exception for the existence of a darker than usual band separating the EZ signal from the signal originating from the tip or distal photoreceptor outer segments as they interdigitate with the apical RPE, conventionally known as the interdigitation zone (IZ) band (60,63). The foveal center in P2 appears to be normal in thickness and the only visible abnormality is the loss of the IZ signal with approximation of the EZ to the apical RPE with an intervening hyporreflective signal. In the juxtafovea there is a brief interruption of the EZ band (Figure 2b, between yellow arrows). The association of polydactyly, obesity, endocrine abnormalities and an outer retinal degeneration was suggestive of Bardet-Biedl syndrome. Genetic testing by Next Generation Sequencing identified two novel variants in the *BBS7* gene segregating in a compound heterozygous state with the phenotype in both patients: p.Val266Glu:c.797 T > A, maternally inherited, predicted to be damaging by both Polyphen-2 and REVEL, and c.1781_1783delCAT, an in-frame deletion of p.Ser594, inherited from their father. Both patients were negative for mutations in *BBS1, BBS2, BBS4, BBS5, BBS9, BBS10, BBS12*, and *ALSM1* genes (Molecular Vision Laboratories, Panel v1). The involvement of other BBS variants was not pursued.

Author Manuscript Author Manuscript Author Manuscript Author Manuscript

Longitudinal changes and structural–functional relationships in BBS7

Structural changes over a 3-year period were clearly detectable on NIR-FAF in P1 with further loss of the signal and both a centripetal and centrifugal expansion of the juxtafoveal annulus of hypoautofluorescence, whereas P2, the younger brother, showed no discernible changes (Figure 2a). The hypoautofluorescent lesion is delineated in both patients by a thin hyperautofluorescent contour. On SD-OCT there was further foveal thinning in P1, the EZ band no longer detectable within the foveal center (Figure 2b). The juxtafoveal regions of hypoautofluorescence on NIR-FAF co-localized with segments on the SD-OCT cross-sections with increased signal scattering posterior to the RPE (Figure 2b, *asterisks*), and intraretinal hyperreflectivities (Figure 2b, *diagonal arrows*), that may reflect intraretinal pigment migration, Muller cell hypertrophy, or changes in reflectivity of degenerating photoreceptors. The transitional zones where the EZ is lost correspond with the hyperautofluorescent boundary line that surrounds the hypoautofluorescent lesions in each patient (Figure 2b, *vertical dash lines*). On follow-up of P1, signals from the apical RPE in the segment with total loss of the inner and outer segment in juxtafoveal nasal retina are substituted by a hyporreflective void, suggesting RPE degeneration and/or loss following the earlier photoreceptor abnormalities (Figure 2b, *arrowhead*). Changes in the younger brother were limited to the foveal center with a narrower EZ-to-RPE/BrM distance 3 years after his initial baseline visit (Figure 2b, *overlaid vertical bars*). In both brothers there were small centrifugal movements of the interruption of the EZ band towards the temporal parafovea (Figure 2b).

The peripheral visual field extent measured with kinetic perimetry and a V-4e target was moderately constricted in both patients, severely constricted to the smallest size I-4e target. Full-field electroretinograms (ffERGs) showed non-detectable cone-mediated signals whereas rod ERGs were ~80% of the normal amplitudes (Figure 3a). Central retinal function assessed with light- and dark-adapted automatic static perimetry revealed abnormally reduced cone-mediated light-adapted sensitivities by at least one log unit across the central retina, except near fixation where sensitivities approached the lower limit of normal (Figure 3b). Contrasting with the normal retina-wide rod functioning by ffERG, there was also definite rod dysfunction across the central in both patients, locally severe in the nasal retina of P1 where sensitivity losses exceeded 2 log units (Figure 3b). In contrast to this central dysfunction, particularly the cone dysfunction by electroretinography, quantitation of the central retinal structure showed a different picture (Figure 3c). The thicknesses of the central ONL, which includes the photoreceptor nuclei and their laterally displaced axonal projections, and of the ‘outer retinal sublaminae’, a term that corresponds to the distance from the photoreceptor inner segment ellipsoid region (conventionally named inner segment ellipsoid band EZ) to the RPE/BrM were comparatively preserved in both patients (Figure 3c) (57,66,67). At the foveal center the ONL thickness was near the lower limit of normal in P2, thinner than normal in P1. The ONL remained at the lower limit of normal or slightly thinner than normal in both patients, with a local dip between 0.5 and 1 mm of the foveal center (Figure 3c).

The modest changes in the overall thickness of the photoreceptor ONL layer in our patients contrasted with the depth of the retinal dysfunction, in particular the severe and retina-wide

Author Manuscript Author Manuscript Author Manuscript Author Manuscript

loss of cone function, prompted exploration of changes of the distal photoreceptors and apical RPE with the use of LRP analyses (Figure 4) (40,62,63,68). LRPs can be used to unambiguously visualize the signal transitions of the OCT cross-sections. In the normal retina major signal troughs correspond to the nuclear layers, while broad hyperscattering signal peaks correspond to the plexiform and retinal nerve fiber layers (Figure 4a). The LRP waveform for these major components have a normal appearance in the BBS7 patients (Figure 4a). A magnified view to the LRP segment distal to the OLM in the normal retina reveals closely spaced hyperscattering peaks that vary in number and position with increasing distance from the foveal center (Figure 4b). (40,58,59,62,63,68–70) The peaks correspond to the ellipsoid region of the photoreceptor inner segments or ellipsoid band (ISe or EZ), the contact cylinder between the apical RPE and the photoreceptor outer segments tips, conventionally termed the interdigitation zone (IZ), and the basal RPE and Bruch's membrane signals (RPE/BrM) (40,58–63,68–73). Within the rod-free foveola the distance between the ISe and the EZ peak, which relates to the length of the cone photoreceptor outer segments, is slightly shorter in P2 with milder changes, but severely shortened in P1 (Figure 4b, *red segment on LRPs*). A short distance from the foveal center in nasal retina of a normal subject illustrates the complexity of the signals. Here the peak that corresponds to the COST/IZ peak at the foveola moves proximally (or superficially) (Figure 4b, *red segment in normal trac*ing), the remaining segment of the LRP to the RPE/BrM peak represents the distal end of the rod photoreceptor outer segment (ROS) (Figure 4b, *i segment in normal trace*). Both patients do not show the peak associated with the cone outer segment signal and the EZ-to-RPE/BrM distance is shorter compared to normal (Figures 4d and 4c). The combination of a moderately thin ONL with obvious outer segment abnormalities for both cone and rod photoreceptors suggests reduced cone photoreceptor densities and the presence of rods with abnormally shorten outer segments, providing an explanation for the sensitivity losses for both photoreceptor mechanisms (Figure 4c).

To further explore the photoreceptor abnormalities AOSLO imaging was performed in both patients (Figure 5 P1, Figure 6 P2). P1 showed a tightly packed inner segment cone mosaic at the foveal center surrounded by a region of cone loss corresponding to the bull's eye lesion (Figure 5). Peak cone density within the foveal region was measured as 31,736 cones/mm^2 which is 27% of normal density (normal foveal density: 119,000 ± 23,300 cones/mm^2)(48). The foveal cones and a pocket of cones at 0.6 mm temporal to the fovea displayed waveguiding of outer segments on confocal AO images, however the retained waveguiding signal appeared mottled and dim in comparison to brightly reflective and Gaussian-shaped profiles of normally waveguiding cones (Figure 5, confocal 0.6 mm Temporal). Cone density in this location was 13,991 cones/mm^2 or approximately 44% of normal density (normal 31,500 cones/mm2). Beyond this location, cone density was further reduced; at 1.3 mm temporal cone density was 21% of normal (3,331 cones/mm^2 compared to 15,800 cones/mm^2) and did not exhibit waveguiding outer segments (Figure 5). Though rods at this location did retain waveguiding outer segments, rod density was reduced to 59,000 rods/mm^2 (normal rod density: 80,000 rods/mm^2) (74–77). RPE density was on the high side of normal at this location and was measured as 6,330 RPE cells/mm. P2 displayed a similar adaptive optics ophthalmoscopy phenotype (Figure 6) as P1. Peak cone density in the fovea was 97,814 cones/mm^2 or 82% of normal. Foveal cones retained normal

Author Manuscript Author Manuscript Author Manuscript Author Manuscript

waveguiding reflectance properties, although there was a small region in the superior-nasal parafovea that displayed a patch of abnormally dim waveguiding cones (Figure 6). The cone inner segment mosaic was intact at this location. Cones at 0.5 mm temporal (Figure 6) were reduced in density (20,186 cones/mm2 or 52% of normal) and displayed the abnormal mottled waveguide appearance described at the same location in P1. Beyond this location, cone density was further reduced and cones did not waveguide (Figure 6). Cone density at 1.9 mm temporal was 2,577 cones/mm2 (22% of normal) and rod density was reduced to 56,262 rods/mm (49% of normal). Overall, adaptive optics imaging showed wide-spread loss of the photoreceptors, with a more advanced phenotype in the cone outer segments than the inner segments.

Discussion

To date, there are only limited descriptions of the retinal phenotype of BBS7. The reported cases have shown a severe juvenile-onset pigmentary retinopathy with non-detectable ERGs or small residual cone ERG signals, invariably interpreted as being within the spectrum of retinitis pigmentosa (32,78–82). In the present study, we describe two brothers from a non-consanguineous family with novel compound heterozygous mutations in *BBS7* who presented in the third decade of life with minimal photophobia and blurred vision in the oldest patient, and with virtually no visual symptoms in his highly myopic brother. Visual acuities were within normal limits and there were only subtle color vision abnormalities. Both brothers had associated systemic abnormalities, more numerous in the youngest brother with subclinical retinal changes, fitting a clinical diagnosis of BBS. The retinal exam was dominated by severe juxtafoveal loss of the photoreceptor outer segments and ONL thinning that worsened within a 3-year interval. Foveolar thinning, while obvious in the oldest subject, was nearly undetectable in P2, the youngest brother. Most interestingly, full-field cone ERGs were non-detectable, which contrasted with modest reductions of rod photoreceptor function, somewhat reminiscent to the pattern observed in achromatopsia(83). Static perimetry showed central cone and rod dysfunction in a pattern that may correspond with the earliest stages of a cone-rod dystrophy(84). This pattern of retina-wide cone>rod ERG abnormalities, while previously unreported for BBS7, is well modelled in the recently described non-human primate model of the disease(35).

Variability of expression of the retinal and systemic abnormalities has long been recognized in BBS, dating back to the pre-molecular era, making BBS an example of pleiotropism (10,14,85). The cases reported herein are encouraging as they suggest a molecular diagnosis of BBS7 should not automatically equate with early and severe vision loss (10–13). They also provide a view into the mildest abnormalities in this specific BBS subtype and thus a possible insight into the pathophysiology of the disease. Of interest, macular changes with severely reduced visual acuities have been documented and nystagmus reported in BBS7, which indicate severe, early central involvement in this specific form of BBS, and suggests a spectrum of severity, with our cases representing the mildest end of the spectrum (33,86,87). In the previously reported cases, a fast and early phase of cone (or central) photoreceptor degeneration may have preceded, with the disease later converging into a severe retinal degeneration indistinguishable from RP, as described in other forms of cone-rod dystrophy (88). Such scenario may explain the different functional classification

Author Manuscript Author Manuscript Author Manuscript Author Manuscript

and apparent discrepancy of the phenotype between our patients and earlier BBS7 reports. Follow up of our cases into the future will help further elucidate this possibility.

The reasons for the initially severe cone dysfunction, milder rod involvement, and relative preservation of the retinal structure in our patients and reported in BBS are unclear and deserves further exploration. The similarities with the recently described NHP model of the disease, however, are extraordinary and deserve mention as they were interpreted as a model of classical RP(35). Both the *BBS7*-NHP model and the BBS7 patients reported herein (and some features reported in the BBS7 literature) show a predominantly central degeneration with significant cone dysfunction (33,35,86,87). Central involvement with bull's eye maculopathies and central atrophic lesions with predominant cone dysfunction have been repeatedly reported in BBS and seem to be regaining attention (11,14–16,89–91). Underrepresentation of the pattern in the BBS literature may result from the extension, as noted above, of a predominant central disease into a retina-wide degeneration, with convergence of an earlier cone>rod phenotype into a severe, retina-wide photoreceptor degeneration involving rods and cones similarly, a sequence that may be better recognized with earlier molecular diagnoses(88). Experimental work suggests there may be greater susceptibility for cone degeneration in certain forms of BBS (BBS3, BBS5, BBS6, BBS8, BBS21) (25,27,92–94). And a recent study reported a cone-rod dystrophy pattern with a very similar phenotype to that described in our patients in several forms of the disease (BBS1, BBS5, BBS6, BBS10, BBS12) with predominance (5/7 patients) of mutations in genes that encode proteins within the chaperonin complex (15). Juxtafoveal changes and relative preservation of the retina with increasing eccentricity was also documented in that series (15). Among the syndromes overlapping manifestations with BBS, Alström syndrome classically shows a severe early cone dysfunction, as well as in *INPP5E*-associated retinopathies, isolated or as part of Joubert syndrome (5,95–100). The severe and early cone dysfunction described in achromatopsia (ACHM) and blue cone monochromatism (BCM), a molecularly heterogenous group of conditions, resembles the severe cone dysfunction of BBS and Alström syndrome, albeit without the severe rod degeneration that accompanies the latter two conditions (73,101,102). Points of contact between the mechanism of these conditions through the function of the BBSome and/or with the unique physiology of the cone photoreceptor may explain the similarities and eventually reveal a common mechanism (71,103).

In BBS there is greater juxtafoveal/parafoveal involvement, at least initially, than there is foveal involvement, which contrasts with the primarily foveolar and minimally progressive disease in ACHM. The reason for the initial regional predilection for the juxtafovea with relative sparing of the foveola observed in BBS, even in cases with a rod-cone pattern of degeneration in BBS, is unknown. One possibility is the additional involvement of rod photoreceptors, which become more numerous immediately outside of the foveal center (74,104). The cases described here had also locally severe RPE depigmentation and loss, including at the foveal center of P2 when local changes were limited to mild shortening of the cone outer segment, a pattern that has been described in BBS, as well as in ACHM. It is possible that the BBS ciliopathy interferes directly or indirectly with processes critical for the interdependent photoreceptors and RPE cells (71,105,106). Using AOSLO we documented severely reduced cone photoreceptor densities all across the central retina and

Author Manuscript Author Manuscript Author Manuscript Author Manuscript

to a similar extent in both patients, independent of the degree of degeneration. The finding may be consistent with an early cone loss phase and/or a developmental failure as proposed for blue cone monochromatism(73). The presence of a relatively intact ONL in the same regions where the loss of the photoreceptor distal organelles was documented by AOSLO suggests relative sparing of the cells, at least for some time, after the loss of the inner and outer segments. Symptomatic presentation may relate to a phase when the disease crosses into a degenerative stage starting with the cells immediately surrounding the foveal center. Determining the factors that lead to this outcome warrants further study.

Restoration of the physiology of a renewable organelle of terminally differentiated neurons, such as the photoreceptor outer segment, makes retinal ciliopathies, including BBS and related conditions, attractive targets for intervention (107,108). There are now several examples of improvements of the retinal and systemic phenotype of several BBS animal models through various approaches, including forms of gene therapy (17,107,109–115). Retinal gene therapy in the bbs1, bbs4, bbs10 and bbs17 mouse models have shown promising structural and functional results, suggesting that proper BBSome complex formation can be restored along with restored ciliary protein trafficking with improved retinal function (108,109,112,113,115). Similarly encouraging results have been demonstrated in the treatment of *NPHP5*- and *CEP290*-associated ciliopathies, which involve proteins intrinsically associated with the BBSome (116,117). The phenotype of the BBS7 siblings described herein include a disproportionate loss of cone and rod vision with relatively preserved photoreceptors. This clinical picture likely represents not a unique phenotype, but rather, a view through a time-window of an otherwise progressive retinal degeneration where interventions may have the best odds at restoring vision, as has been already demonstrated in proof-of-concept experimental studies in BBS and in patients with early and severe inherited retinal degenerations (108,118–123). Although proof-of-concept treatments for BBS7 disease do not exist today, the possibility of variations of the BBS7 phenotype described herein exists. This, together with the availability of the BBS7 NHP animal model of the disease, provide the needed motivations for developing future interventions for BBS7(35). Thus, despite the low prevalence of BBS7 as a cause of BBS, the important role of the protein in the pathophysiology of the much larger group of retinal ciliopathies as well as the existence of an ideal animal model, position BBS7 as an ideal target for experimental treatments that will both, increase our understanding of these conditions and ultimately move treatments into the clinic for patients suffering from these complex syndromes (17,18,86).

Acknowledgments

We thank the family who participated in this research. We also thank Alfredo Dubra and Min Chen. Dr. E.C. O'Neil is a recipient of the Diana Davis Spencer Clinical/Research Fellowship Award Program in Inherited Retinal Degenerations within FFB's Alan Laties Career Development Program. Additional support is from grants from Hope for Vision, Macula Vision Research Foundation and The Pennsylvania Lions Sight Conservation and Research Foundation. Foundation Fighting Blindness (BR-CL-0619–0768-UPA), Research to Prevent Blindness Stein Innovation Award, and National Eye Institute, National Institute of Health (NEI, NIH) (P30 EY001583, R01 EY028601, R01 EY030227), and the F. M. Kirby Foundation; and the Paul and Evanina Mackall Foundation Trust.

Author Manuscript Author Manuscript Author Manuscript Author Manuscript

Funding

This work was supported by the Hope For Vision; F. M. Kirby Foundation; and the Paul and Evanina Mackall Foundation Trust; The Pennsylvania Lions Sight Conservation and Research Foundation; Foundation Fighting Blindness; National Eye Institute, National Institute of Health [P30 EY001583, R01 EY028601, R01 EY030227]; Diana Davis Spencer Clinical/Research Fellowship Award Program in Inherited Retinal Degenerations within FFB's Alan Laties Career Development Program; Research to Prevent Blindness Stein Innovation Award; Macula Vision Research Foundation.

References

1. Krill AE, Folk E, Rosenthal IM. Electroretinography in the Laurence-Moon-Biedl syndrome. An aid in diagnosis of the atypical case. Am J Dis Child. 1961;102:205–09. doi:10.1001/archpedi.1961.02080010207009. [PubMed: 13754342]
2. Green JS, Parfrey PS, Harnett JD, Farid NR, Cramer BC, Johnson G, Heath O, McManamon PJ, O'Leary E, Pryse-Phillips W, et al. The cardinal manifestations of Bardet-Biedl syndrome, a form of Laurence-Moon-Biedl syndrome. N Engl J Med. 1989;321:1002–09. [PubMed: 2779627]
3. Forsyth RL, Gunay-Aygun M. Bardet-Biedl Syndrome Overview. 2003 7 14 [Updated 2020 Jul 23]. In: Adam MP, Ardinger HH, Pagon RA, et al., editors. GeneReviews® [Internet]. Seattle (WA): University of Washington, Seattle; 1993–2021. Available from: https://www-ncbi-nlm-nih-gov.proxy.library.upenn.edu/books/NBK1363/.
4. Badano JL, Ansley SJ, Leitch CC, Lewis RA, Lupski JR, Katsanis N. Identification of a novel Bardet-Biedl syndrome protein, BBS7, that shares structural features with BBS1 and BBS2. Am J Hum Genet. 2003;72:650–58. doi:10.1086/368204. [PubMed: 12567324]
5. Weihbrecht K, Goar WA, Pak T, Garrison JE, DeLuca AP, Stone EM, Scheetz TE, Sheffield VC. Keeping an eye on bardet-biedl syndrome: a comprehensive review of the role of bardet-biedl syndrome genes in the eye. Med Res Arch. 2017;5. doi:10.18103/mra.v18105i18109.11526.
6. Forsythe E, Beales PL. Bardet-Biedl syndrome. Eur J Hum Genet. 2013;21:8–13. doi:10.1038/ejhg.2012.115. [PubMed: 22713813]
7. Bardet G Sur un syndrome d'obésité congénitale avec polydactylie et rétinite pigmentaire (contribution à l'étude des formes cliniques de l'obésité hypophysaire). Université de Paris, Thesis no 470, Legrand; 1920.
8. Biedl A. Ein Geschwisterpaar mit adiposo-genitaler Dystrophie. Dtsch Med Wochenschr. 1922;48:1630.
9. Laurence JZ, Moon RC. Four cases of 'retinitis pigmentosa', occurring in the same family, and accompanied by general imperfections of development. Ophthalmic Rev (Old Series). 1866;2:32–41.
10. Denniston AK, Beales PL, Tomlins PJ, Good P, Langford M, Foggensteiner L, Williams D, Tsaloumas MD. Evaluation of visual function and needs in adult patients with bardet-biedl syndrome. Retina. 2014;34:2282–89. [PubMed: 25170860]
11. Mockel A, Perdomo Y, Stutzmann F, Letsch J, Marion V, Dollfus H. Retinal dystrophy in Bardet-Biedl syndrome and related syndromic ciliopathies. Prog Retin Eye Res. 2011;30:258–74. doi:10.1016/j.preteyeres.2011.03.001. [PubMed: 21477661]
12. Berezovsky A, Rocha DM, Sacai PY, Watanabe SS, Cavascan NN, Salomao SR. Visual acuity and retinal function in patients with Bardet-Biedl syndrome. Clinics (Sao Paulo). 2012;67:145–49. doi:10.6061/clinics/2012(02)09.
13. Fulton AB, Hansen RM, Glynn RJ. Natural course of visual functions in the Bardet-Biedl syndrome. Arch Ophthalmol. 1993;111:1500–06. doi:10.1001/archopht.1993.01090110066026. [PubMed: 8240105]
14. Azari AA, Aleman TS, Cideciyan AV, Schwartz SB, Windsor EAM, Sumaroka A, Cheung AY, Steinberg JD, Roman AJ, Stone EM, et al. Retinal disease expression in bardet-biedl syndrome-1 (BBS1) is a spectrum from maculopathy to retina-wide degeneration. Invest Ophthalmol Vis Sci. 2006;47:5004–10. [PubMed: 17065520]
15. Scheidecker S, Hull S, Perdomo Y, Studer F, Pelletier V, Muller J, Stoetzel C, Schaefer E, Defoort-Dhellemmes S, Drumare I, et al. Predominantly cone-system dysfunction as rare form of retinal

Author Manuscript Author Manuscript Author Manuscript Author Manuscript

degeneration in patients with molecularly confirmed bardet-biedl syndrome. Am J Ophthalmol. 2015;160:364–372e361. [PubMed: 25982971]

16. Jacobson SG, Borruat FX, Apathy PP. Patterns of rod and cone dysfunction in Bardet-Biedl syndrome. Am J Ophthalmol. 1990;109:676–88. doi:10.1016/S0002-9394(14)72436-5. [PubMed: 2346197]
17. Forsythe E, Kenny J, Bacchelli C, Beales PL. Managing Bardet-Biedl syndrome-now and in the future. Front Pediatr. 2018;6:23. doi:10.3389/fped.2018.00023. [PubMed: 29487844]
18. Khan SA, Muhammad N, Khan MA, Kamal A, Rehman ZU, Khan S. Genetics of human Bardet-Biedl syndrome, an updates. Clin Genet. 2016;90:3–15. doi:10.1111/cge.12737. [PubMed: 26762677]
19. Badano JL, Kim JC, Hoskins BE, Lewis RA, Ansley SJ, Cutler DJ, Castellan C, Beales PL, Leroux MR, Katsanis N. Heterozygous mutations in BBS1, BBS2 and BBS6 have a potential epistatic effect on Bardet-Biedl patients with two mutations at a second BBS locus. Hum Mol Genet. 2003 7 15;12(14):1651–9. doi:10.1093/hmg/ddg188. [PubMed: 12837689]
20. Blacque OE, Reardon MJ, Li C, McCarthy J, Mahjoub MR, Ansley SJ, Badano JL, Mah AK, Beales PL, Davidson WS, et al. Loss of C. elegans BBS-7 and BBS-8 protein function results in cilia defects and compromised intraflagellar transport. Genes Dev. 2004 7 1;18(13):1630–42. doi:10.1101/gad.1194004. [PubMed: 15231740]
21. Blacque OE, Leroux MR. Bardet-Biedl syndrome: an emerging pathomechanism of intracellular transport. Cell Mol Life Sci. 2006;63:2145–61. doi:10.1007/s00018-006-6180-x. [PubMed: 16909204]
22. Aldahmesh MA, Li Y, Alhashem A, Anazi S, Alkuraya H, Hashem M, Awaji AA, Sogaty S, Alkharashi A, Alzahrani S, et al. IFT27, encoding a small GTPase component of IFT particles, is mutated in a consanguineous family with Bardet-Biedl syndrome. Hum Mol Genet. 2014;23:3307–15. [PubMed: 24488770]
23. Prasai A, Schmidt Cernohorska M, Ruppova K, Niederlova V, Andelova M, Draber P, Stepanek O, Huranova M. The BBSome assembly is spatially controlled by BBS1 and BBS4 in human cells. J Biol Chem. 2020;295(42):14279–90. doi:10.1074/jbc.RA120.013905. [PubMed: 32759308]
24. Zhang Q, Yu D, Seo S, Stone EM, Sheffield VC. Intrinsic protein-protein interaction-mediated and chaperonin-assisted sequential assembly of stable bardet-biedl syndrome protein complex, the BBSome. J Biol Chem. 2012;287:20625–35. doi:10.1074/jbc.M112.341487. [PubMed: 22500027]
25. Bales KL, Bentley MR, Croyle MJ, Kesterson RA, Yoder BK, Gross AK. BBSome component BBS5 is required for cone photoreceptor protein trafficking and outer segment maintenance. Invest Ophthalmol Vis Sci. 2020;61:17. doi:10.1167/iovs.61.10.17.
26. Zhang Q, Nishimura D, Vogel T, Shao J, Swiderski R, Yin T, Searby C, Carter CS, Kim G, Bugge K, et al. BBS7 is required for BBSome formation and its absence in mice results in Bardet-Biedl syndrome phenotypes and selective abnormalities in membrane protein trafficking. J Cell Sci. 2013;126:2372–80. [PubMed: 23572516]
27. Kretschmer V, Patnaik SR, Kretschmer F, Chawda MM, Hernandez-Hernandez V, May-Simera HL. Progressive characterization of visual phenotype in bardet-biedl syndrome mutant mice. Invest Ophthalmol Vis Sci. 2019;60:1132–43. doi:10.1167/iovs.18-25210. [PubMed: 30901771]
28. Seo S, Baye LM, Schulz NP, Beck JS, Zhang Q, Slusarski DC, Sheffield VC. BBS6, BBS10, and BBS12 form a complex with CCT/TRiC family chaperonins and mediate BBSome assembly. Proc Natl Acad Sci U S A. 2010;107:1488–93. [PubMed: 20080638]
29. Datta P, Allamargot C, Hudson JS, Andersen EK, Bhattarai S, Drack AV, Sheffield VC, Seo S. Accumulation of non-outer segment proteins in the outer segment underlies photoreceptor degeneration in Bardet-Biedl syndrome. Proc Natl Acad Sci U S A. 2015;112:E4400–4409. [PubMed: 26216965]
30. Feuillan PP, Ng D, Han JC, Sapp JC, Wetsch K, Spaulding E, Zheng YC, Caruso RC, Brooks BP, Johnston JJ, et al. Patients with Bardet-Biedl syndrome have hyperleptinemia suggestive of leptin resistance. J Clin Endocrinol Metab. 2011;96:E528–535. [PubMed: 21209035]
31. Shen T, Gao JM, Shou T, Li L, Zhang J-P, Zhao Q, Yan X-M. Identification of a homozygous BBS7 frameshift mutation in two (related) Chinese Miao families with Bardet-Biedl Syndrome. J Chin Med Assoc. 2019;82:110–14. [PubMed: 30839500]

Author Manuscript Author Manuscript Author Manuscript Author Manuscript

32. Hayat A, Khan AA, Rauf A, Khan SU, Hussain S, Ullah A, Ahmad W, Shams S, Khan B. A novel missense variant in the BBS7 gene underlying Bardet-Biedl syndrome in a consanguineous Pakistani family. Clin Dysmorphol. 2020;29:17–23. [PubMed: 31469663]
33. Yang Z, Yang Y, Zhao P, Chen K, Chen B, Lin Y, Guo F, Chen Y, Liu X, Lu F, et al. A novel mutation in BBS7 gene causes Bardet-Biedl syndrome in a Chinese family. Mol Vis. 2008;14:2304–08. [PubMed: 19093007]
34. Niederlova V, Modrak M, Tsyklauri O, Huranova M, Stepanek O. Meta-analysis of genotype-phenotype associations in Bardet-Biedl syndrome uncovers differences among causative genes. Hum Mutat. 2019;40:2068–87. doi:10.1002/humu.23862. [PubMed: 31283077]
35. Peterson SM, McGill TJ, Puthussery T, Stoddard J, Renner L, Lewis AD, Colgin LMA, Gayet J, Wang X, Prongay K, et al. Bardet-Biedl Syndrome in rhesus macaques: a nonhuman primate model of retinitis pigmentosa. Exp Eye Res. 2019;189:107825. [PubMed: 31589838]
36. Jacobson S, Voigt W, Parel J-M, Apathy PP, Nghiem-Phu L, Myers SW, Patella VM. Automated light- and dark-adapted perimetry for evaluating retinitis pigmentosa. Ophthalmology. 1986;93:1604–11. [PubMed: 3808619]
37. Aleman TS, Han G, Serrano LW, Fuerst NM, Charlson ES, Pearson DJ, Chung DC, Traband A, Pan W, Ying G-S, et al. Natural history of the central structural abnormalities in choroideremia: a prospective cross-sectional study. Ophthalmology. 2017;124:359–73. [PubMed: 27986385]
38. McCulloch DL, Marmor MF, Brigell MG, Hamilton R, Holder GE, Tzekov R, Bach M. ISCEV Standard for full-field clinical electroretinography (2015 update). Doc Ophthalmol. 2015;130:1–12.
39. Ammar MJ, Scavelli KT, Uyhazi KE, Bedoukian EC, Serrano LW, Edelstein ID, Vergilio G, Cooper RF, Morgan JIW, Kumar P, et al. Enhanced S-cone syndrome: visual function, cross-sectional imaging, and cellular structure with adaptive optics ophthalmoscopy. Retin Cases Brief Rep;2019. doi:10.1097/ICB.0000000000000891. Epub ahead of print.
40. Huang Y, Cideciyan AV, Papastergiou GI, Banin E, Semple-Rowland SL, Milam AH, Jacobson SG. Relation of optical coherence tomography to microanatomy in normal and rd chickens. Invest Ophthalmol Vis Sci. 1998;39:2405–16. [PubMed: 9804149]
41. Dubra A, Sulai Y. Reflective afocal broadband adaptive optics scanning ophthalmoscope. Biomed Opt Express. 2011;2:1757. doi:10.1364/BOE.2.001757. [PubMed: 21698035]
42. Scoles D, Sulai YN, Langlo CS, Fishman GA, Curcio CA, Carroll J, Dubra A. In vivo imaging of human cone photoreceptor inner segments. Investigative Opthalmology & Visual Science. 2014;55:4244.
43. Dubra A, Harvey Z. Registration of 2D images from fast scanning ophthalmic instruments. Lect Notes Comput Sci. 2010;6204:60–71.
44. Dubra A, Sulai Y, Norris JL, Cooper RF, Dubis AM, Williams DR, Carroll J. Noninvasive imaging of the human rod photoreceptor mosaic using a confocal adaptive optics scanning ophthalmoscope. Biomed Opt Express. 2011;2:1864–76. [PubMed: 21750765]
45. Salmon AE, Cooper RF, Langlo CS, Baghaie A, Dubra A, Carroll J. An automated reference frame selection (ARFS) algorithm for cone imaging with adaptive optics scanning light ophthalmoscopy. Transl Vis Sci Technol. 2017;6:9. doi:10.1167/tvst.6.2.9.
46. Chen M, Cooper RF, Gee JC, Brainard DH, Morgan JIW. Automatic longitudinal montaging of adaptive optics retinal images using constellation matching. Biomed Opt Express. 2019;10:6476–96. doi:10.1364/BOE.10.006476. [PubMed: 31853412]
47. Chen M, Cooper RF, Han GK, Gee J, Brainard DH, Morgan JIW. Multi-modal automatic montaging of adaptive optics retinal images. Biomed Opt Express. 2016;7:4899–918. doi:10.1364/BOE.7.004899. [PubMed: 28018714]
48. Cooper RF, Wilk MA, Tarima S, Carroll J. Evaluating descriptive metrics of the human cone mosaic. Investigative Opthalmology & Visual Science. 2016;57:2992. doi:10.1167/iovs.16-19072.
49. Garrioch R, Langlo C, Dubis AM, Cooper RF, Dubra A, Carroll J. Repeatability of in vivo parafoveal cone density and spacing measurements. Optom Vis Sci. 2012;89:632–43. doi:10.1097/OPX.0b013e3182540562. [PubMed: 22504330]

Author Manuscript Author Manuscript Author Manuscript Author Manuscript

50. Keilhauer CN, Delori FC. Near-infrared autofluorescence imaging of the fundus: visualization of ocular melanin. Invest Ophthalmol Vis Sci. 2006;47:3556–64. doi:10.1167/iovs.06-0122. [PubMed: 16877429]
51. Aleman TS, Cideciyan AV, Windsor EA, Schwartz SB, Swider M, Chico JD, Sumaroka A, Pantelyat AY, Duncan KG, Gardner LM, et al. Macular pigment and lutein supplementation in ABCA4 - associated retinal degenerations. Invest Ophthalmol Vis Sci. 2007;48:1319–29. [PubMed: 17325179]
52. Cideciyan A, Swider M, Aleman T, Roman M, Sumaroka A, Schwartz S. Reduced-illuminance autofluorescence imaging in ABCA4-associated retinal degenerations. J Opt Soc Am A. 2007;24:1457–67. doi:10.1364/JOSAA.24.001457.
53. Hammond BR Jr., Wooten BR, Snodderly DM. Individual variations in the spatial profile of human macular pigment. J Opt Soc Am A Opt Image Sci Vis. 1997;14:1187–96. doi:10.1364/JOSAA.14.001187. [PubMed: 9168592]
54. Ctori I, Huntjens B. The association between foveal morphology and macular pigment spatial distribution: an ethnicity study. PLoS One. 2017;12:e0169520. doi:10.1371/journal.pone.0169520. [PubMed: 28068388]
55. Delori FC, Goger DG, Keilhauer C, Salvetti P, Staurenghi G. Bimodal spatial distribution of macular pigment: evidence of a gender relationship. J Opt Soc Am A Opt Image Sci Vis. 2006;23:521–38. doi:10.1364/JOSAA.23.000521. [PubMed: 16539047]
56. Berendschot TT, van Norren D. Macular pigment shows ringlike structures. Invest Ophthalmol Vis Sci. 2006;47:709–14. doi:10.1167/iovs.05-0663. [PubMed: 16431971]
57. Lujan BJ, Roorda A, Knighton RW, Carroll J. Revealing Henle's fiber layer using spectral domain optical coherence tomography. Invest Ophthalmol Vis Sci. 2011;52:1486–92. doi:10.1167/iovs.10-5946. [PubMed: 21071737]
58. Jonnal RS, Besecker JR, Derby JC, Kocaoglu OP, Cense B, Gao W, Wang Q, Miller DT. Imaging outer segment renewal in living human cone photoreceptors. Opt Express. 2010;18:5257–70. [PubMed: 20389538]
59. Jonnal RS, Kocaoglu OP, Zawadzki RJ, Lee S-H, Werner JS, Miller DT. The cellular origins of the outer retinal bands in optical coherence tomography images. Invest Ophthalmol Vis Sci. 2014;55:7904–18. doi:10.1167/iovs.14-14907. [PubMed: 25324288]
60. Staurenghi G, Sadda S, Chakravarthy U, Spaide RF. International nomenclature for optical coherence tomography P. Proposed lexicon for anatomic landmarks in normal posterior segment spectral-domain optical coherence tomography: the IN•OCT consensus. Ophthalmology. 2014;121:1572–78. doi:10.1016/j.ophtha.2014.02.023. [PubMed: 24755005]
61. Cuenca N, Ortuño-Lizarán I, Pinilla I. Cellular characterization of OCT and outer retinal bands using specific immunohistochemistry markers and clinical implications. Ophthalmology. 2018;125:407–22. doi:10.1016/j.ophtha.2017.09.016. [PubMed: 29037595]
62. Huang Y, Cideciyan A, Aleman T, Banin E, Huang J, Syed NA, Petters RM, Wong F, Milam AH, Jacobson SG, et al. Optical coherence tomography (OCT) abnormalities in rhodopsin mutant transgenic swine with retinal degeneration. Exp Eye Res. 2000;70:247–51. [PubMed: 10655151]
63. Nti AA, Serrano LW, Sandhu HS, Uyhazi KE, Edelstein ID, Zhou EJ, Bowman S, Song D, Gangadhar TC, Schuchter LM, et al. Frequent subclinical macular changes in combined BRAF/MEKinhibition with high-dose hydroxychloroquine as treatment for advanced BRAF mutant melanoma: preliminary results from a phase I/II clinical treatment trial. Retina. 2019;39:502–13. [PubMed: 29324592]
64. Hogan MJ, Alvarado JA, Weddell JE. Retina. In: Histology of the human eye: an atlas and textbook. Saunders; 1971.
65. Kolb H, Nelson RF, Ahnelt PK, Ortuno-Lizaran I, Cuenca N. The architecture of the human fovea. In: Kolb H, Fernandez E, Nelson R, editors. Webvision: the organization of the retina and visual system. Salt Lake City (UT); 1995.
66. Drasdo N, Millican CL, Katholi CR, Curcio CA. The length of Henle fibers in the human retina and a model of ganglion receptive field density in the visual field. Vision Res. 2007;47:2901–11. doi:10.1016/j.visres.2007.01.007. [PubMed: 17320143]

Author Manuscript Author Manuscript Author Manuscript Author Manuscript

67. Aleman TS, Uyhazi KE, Serrano LW, Vasireddy V, Bowman SJ, Ammar MJ, Pearson DJ, Maguire AM, Bennett J. *RDH12* mutations cause a severe retinal degeneration with relatively spared rod function. Invest Ophthalmol Vis Sci. 2018;59:5225–36. [PubMed: 30372751]
68. Aleman TS, Ventura CV, Cavalcanti MM, Serrano LW, Traband A, Nti AA, Gois AL, Bravo-Filho V, Martins TT, Nichols CW, et al. Quantitative assessment of microstructural changes of the retina in infants with congenital Zika syndrome. JAMA Ophthalmol. 2017;135:1069–76. [PubMed: 28880978]
69. Srinivasan VJ, Monson BK, Wojtkowski M, Bilonick RA, Gorczynska I, Chen R, Duker JS, Schuman JS, Fujimoto JG. Characterization of outer retinal morphology with high-speed, ultrahigh-resolution optical coherence tomography. Invest Ophthalmol Vis Sci. 2008;49:1571–79. [PubMed: 18385077]
70. Kocaoglu OP, Lee S, Jonnal RS, Wang Q, Herde AE, Derby JC, Gao W, Miller DT. Imaging cone photoreceptors in three dimensions and in time using ultrahigh resolution optical coherence tomography with adaptive optics. Biomed Opt Express. 2011;2:748. [PubMed: 21483600]
71. Mustafi D, Kevany BM, Genoud C, Okano K, Cideciyan AV, Sumaroka A, Roman AJ, Jacobson SG, Engel A, Adams MD, et al. Defective photoreceptor phagocytosis in a mouse model of enhanced S-cone syndrome causes progressive retinal degeneration. Faseb J. 2011;25:3157–76. [PubMed: 21659555]
72. Spaide RF, Curcio CA. Anatomical correlates to the bands seen in the outer retina by optical coherence tomography: literature review and model. Retina. 2011;31:1609–19. doi:10.1097/IAE.0b013e3182247535. [PubMed: 21844839]
73. Cideciyan AV, Hufnagel RB, Carroll J, Sumaroka A, Luo X, Schwartz SB, Dubra A, Land M, Michaelides M, Gardner JC, et al. Human cone visual pigment deletions spare sufficient photoreceptors to warrant gene therapy. Hum Gene Ther. 2013;24:993–1006. [PubMed: 24067079]
74. Curcio CA, Sloan KR, Kalina RE, Hendrickson AE. Human photoreceptor topography. J Comp Neurol. 1990;292:497–523. doi:10.1002/cne.902920402. [PubMed: 2324310]
75. Morgan JI, Dubra A, Wolfe R, Merigan WH, Williams DR. In vivo autofluorescence imaging of the human and macaque retinal pigment epithelial cell mosaic. Invest Ophthalmol Vis Sci. 2009;50:1350–59. doi:10.1167/iovs.08-2618. [PubMed: 18952914]
76. Scoles D, Sulai YN, Dubra A. In vivo dark-field imaging of the retinal pigment epithelium cell mosaic. Biomed Opt Express. 2013;4:1710–23. doi:10.1364/BOE.4.001710. [PubMed: 24049692]
77. Granger CE, Yang Q, Song H, Saito K, Nozato K, Latchney LR, Leonard BT, Chung MM, Williams DR, Rossi EA, et al. Human retinal pigment epithelium: in vivo cell morphometry, multispectral autofluorescence, and relationship to cone mosaic. Invest Ophthalmol Vis Sci. 2018;59:5705–16. [PubMed: 30513531]
78. Harville HM, Held S, Diaz-Font A, Davis EE, Diplas BH, Lewis RA, Borochowitz ZU, Zhou W, Chaki M, MacDonald J, et al. Identification of 11 novel mutations in eight BBS genes by high-resolution homozygosity mapping. J Med Genet. 2010;47:262–67. [PubMed: 19797195]
79. Janssen S, Ramaswami G, Davis EE, Hurd T, Airik R, Kasanuki JM, Van Der Kraak L, Allen SJ, Beales PL, Katsanis N, et al. Mutation analysis in Bardet-Biedl syndrome by DNA pooling and massively parallel resequencing in 105 individuals. Hum Genet. 2011;129:79–90. [PubMed: 21052717]
80. Daniels AB, Sandberg MA, Chen J, Weigel-DiFranco C, Fielding Hejtmancic J, Berson EL. Genotype-phenotype correlations in Bardet-Biedl syndrome. Arch Ophthalmol. 2012;130:901–07. doi:10.1001/archophthalmol.2012.89. [PubMed: 22410627]
81. Shin SJ, Kim M, Chae H, Kwon A, Kim Y, Kim SJ, Yoon HE, Jekarl DW, Lee S. Identification of compound heterozygous mutations in the BBS7 gene in a Korean family with bardet-biedl syndrome. Ann Lab Med. 2015;35:181–84. [PubMed: 25553308]
82. Shaukat M, Ishaq T, Muhammad N, Naz S. RIN2 and BBS7 variants as cause of a coincidental syndrome. Eur J Med Genet. 2020;63:103755. doi:10.1016/j.ejmg.2019.103755. [PubMed: 31521835]
83. Kohl S, Jägle H, Wissinger B, Zobor D. Achromatopsia. 2004 6 24 [updated 2018 Sep 20]. In: Adam MP, Ardinger HH, Pagon RA, Wallace SE, Bean LJH, Stephens K, Amemiya A, editors. GeneReviews® [Internet]. Seattle (WA): University of Washington, Seattle; 1993–2020.

Author Manuscript Author Manuscript Author Manuscript Author Manuscript

84. Gill JS, Georgiou M, Kalitzeos A, Moore AT, Michaelides M. Progressive cone and cone-rod dystrophies: clinical features, molecular genetics and prospects for therapy. Br J Ophthalmol. 2019;103:711–20. doi:10.1136/bjophthalmol-2018-313278.
85. Riise R, Andreasson S, Borgastrom MK, Wright AF, Tommerup N, Rosenberg T, Tornqvist K. Intrafamilial variation of the phenotype in Bardet-Biedl syndrome. Br J Ophthalmol. 1997;81:378–85. [PubMed: 9227203]
86. Bin J, Madhavan J, Ferrini W, Mok CA, Billingsley G, Heon E. BBS7 and TTC8 (BBS8) mutations play a minor role in the mutational load of Bardet-Biedl syndrome in a multiethnic population. Hum Mutat. 2009;30:E737–746. doi:10.1002/humu.21040. [PubMed: 19402160]
87. Ece Solmaz A, Onay H, Atik T, Aykut A, Cerrah Gunes M, Ozalp Yuregir O, Bas VN, Hazan F, Kirbiyik O, Ozkinay F, et al. Targeted multi-gene panel testing for the diagnosis of Bardet Biedl syndrome: identification of nine novel mutations across BBS1, BBS2, BBS4, BBS7, BBS9, BBS10 genes. Eur J Med Genet. 2015;58:689–94. [PubMed: 26518167]
88. Matsui R, McGuigan Iii DB, Gruzensky ML, Aleman TS, Schwartz SB, Sumaroka A, Koenekoop RK, Cideciyan AV, Jacobson SG. SPATA7 : evolving phenotype from cone-rod dystrophy to retinitis pigmentosa. Ophthalmic Genet. 2016;37:333–38. [PubMed: 26854980]
89. Berson EL, Gouras P, Gunkel RD. Progressive cone-rod degeneration. Arch Ophthalmol. 1968;80:68–76. doi:10.1001/archopht.1968.00980050070010. [PubMed: 5660020]
90. Iannaccone A, Vingolo EM, Rispoli E, De Propris G, Tanzilli P, Pannarale MR. Electroretinographic alterations in the Laurence-Moon-Bardet-Biedl phenotype. Acta Ophthalmol Scand. 1996;74:8–13. doi:10.1111/j.1600-0420.1996.tb00673.x. [PubMed: 8689489]
91. Hamel CP. Cone rod dystrophies. Orphanet J Rare Dis. 2007;2:7. doi:10.1186/1750-1172-2-7. [PubMed: 17270046]
92. Dilan TL, Singh RK, Saravanan T, Moye A, Goldberg AFX, Stoilov P, Ramamurthy V. Bardet-Biedl syndrome-8 (BBS8) protein is crucial for the development of outer segments in photoreceptor neurons. Hum Mol Genet. 2018;27:283–94. [PubMed: 29126234]
93. Estrada-Cuzcano A, Koenekoop RK, Senechal A, De Baere EBW, de Ravel T, Banfi S, Kohl S, Ayuso C, Sharon D, Hoyng CB, et al. BBS1 mutations in a wide spectrum of phenotypes ranging from nonsyndromic retinitis pigmentosa to Bardet-Biedl syndrome. Arch Ophthalmol. 2012;130:1425–32. [PubMed: 23143442]
94. Estrada-Cuzcano A, Neveling K, Kohl S, Banin E, Rotenstreich Y, Sharon D, Falik-Zaccai T, Hipp S, Roepman R, Wissinger B, et al. Mutations in C8orf37, encoding a ciliary protein, are associated with autosomal-recessive retinal dystrophies with early macular involvement. Am J Hum Genet. 2012;90:102–09. [PubMed: 22177090]
95. Alstrom CH, Hallgren B, Nilsson LB, Asander H. Retinal degeneration combined with obesity, diabetes mellitus and neurogenous deafness: a specific syndrome (not hitherto described) distinct from the Laurence-Moon-Bardet-Biedl syndrome: a clinical, endocrinological and genetic examination based on a large pedigree. Acta Psychiatr Neurol Scand Suppl. 1959;129:1–35. [PubMed: 13649370]
96. Brooks BP, Zein WM, Thompson AH, Mokhtarzadeh M, Doherty DA, Parisi M, Glass IA, Malicdan MC, Vilboux T, Vemulapalli M, et al. Joubert syndrome: ophthalmological findings in correlation with genotype and hepatorenal disease in 99 patients prospectively evaluated at a single center. Ophthalmology. 2018;125:1937–52. [PubMed: 30055837]
97. Birtel J, Eisenberger T, Gliem M, Müller PL, Herrmann P, Betz C, Zahnleiter D, Neuhaus C, Lenzner S, Holz FG, et al. Clinical and genetic characteristics of 251 consecutive patients with macular and cone/cone-rod dystrophy. Sci Rep. 2018;8(1):4824. doi:10.1038/s41598-018-22096-0. [PubMed: 29555955]
98. Nasser F, Weisschuh N, Maffei P, Milan G, Heller C, Zrenner E, Kohl S, Kuehlewein L. Ophthalmic features of cone-rod dystrophy caused by pathogenic variants in the ALMS1 gene. Acta Ophthalmol. 2018;96(4):e445–e454. doi:10.1111/aos.13612. [PubMed: 29193673]
99. Tremblay F, LaRoche RG, Shea SE, Ludman MD. Longitudinal study of the early electroretinographic changes in Alstrom's syndrome. Am J Ophthalmol. 1993;115:657–65. doi:10.1016/S0002-9394(14)71466-7. [PubMed: 8488920]

Author Manuscript Author Manuscript Author Manuscript Author Manuscript

100. Mauring L, Porter LF, Pelletier V, Riehm A, Leuvrey A-S, Gouronc A, Studer F, Stoetzel C, Dollfus H, Muller J, et al. Atypical retinal phenotype in a patient with alström syndrome and biallelic novel pathogenic variants in ALMS1, including a de novo variation. Front Genet. 2020;11:938. [PubMed: 32973878]

101. Collin GB, Cyr E, Bronson R, Marshall JD, Gifford EJ, Hicks W, Murray SA, Zheng QY, Smith RS, Nishina PM, et al. Alms1-disrupted mice recapitulate human Alstrom syndrome. Hum Mol Genet. 2005;14:2323–33. [PubMed: 16000322]

102. Zelinger L, Cideciyan AV, Kohl S, Schwartz SB, Rosenmann A, Eli D, Sumaroka A, Roman AJ, Luo X, Brown C, et al. Genetics and disease expression in the CNGA3 form of achromatopsia. Ophthalmology. 2015;122(5):997–1007. doi:10.1016/j.ophtha.2014.11.025. [PubMed: 25616768]

103. Mustafi D, Engel AH, Palczewski K. Structure of cone photoreceptors. Prog Retin Eye Res. 2009;28:289–302. doi:10.1016/j.preteyeres.2009.05.003. [PubMed: 19501669]

104. Curcio CA, Allen KA, Sloan KR, Lerea CL, Hurley JB, Klock IB, Milam AH. Distribution and morphology of human cone photoreceptors stained with anti-blue opsin. J Comp Neurol. 1991;312:610–24. [PubMed: 1722224]

105. Sparrrow J R, Hicks D, Hamel C P The retinal pigment epithelium in health and disease. Curr Mol Med. 2010;10:802–23. doi:10.2174/156652410793937813. [PubMed: 21091424]

106. Kevany BM, Palczewski K. Phagocytosis of retinal rod and cone photoreceptors. Physiology (Bethesda). 2010;25:8–15. doi:10.1152/physiol.00038.2009. [PubMed: 20134024]

107. Kenny J, Forsythe E, Beales P, Bacchelli C. Toward personalized medicine in Bardet-Biedl syndrome. Per Med. 2017;14:447–56. doi:10.2217/pme-2017-0019. [PubMed: 29754569]

108. Datta P, Ruffcorn A, Seo S. Limited time window for retinal gene therapy in a preclinical model of ciliopathy. Hum Mol Genet. 2020;29:2337–52. doi:10.1093/hmg/ddaa124. [PubMed: 32568387]

109. Simons DL, Boye SL, Hauswirth WW, Wu SM. Gene therapy prevents photoreceptor death and preserves retinal function in a Bardet-Biedl syndrome mouse model. Proc Natl Acad Sci U S A. 2011;108:6276–81. doi:10.1073/pnas.1019222108. [PubMed: 21444805]

110. Schmid F, Glaus E, Barthelmes D, Fliegauf M, Gaspar H, Nürnberg G, Nürnberg P, Omran H, Berger W, Neidhardt J, et al. U1 snRNA-mediated gene therapeutic correction of splice defects caused by an exceptionally mild BBS mutation. Hum Mutat. 2011;32:815–24. [PubMed: 21520335]

111. Mockel A, Obringer C, Hakvoort TBM, Seeliger M, Lamers WH, Stoetzel C, Dollfus H, Marion V. Pharmacological modulation of the retinal unfolded protein response in Bardet-Biedl syndrome reduces apoptosis and preserves light detection ability. J Biol Chem. 2012;287(44):37483–94. doi:10.1074/jbc.M112.386821. [PubMed: 22869374]

112. Chamling X, Seo S, Bugge K, Searby C, Guo DF, Drack AV, Rahmouni K, Sheffield VC. Ectopic expression of human BBS4 can rescue Bardet-Biedl syndrome phenotypes in Bbs4 null mice. PLoS One. 2013;8(3):e59101. doi:10.1371/journal.pone.0059101. [PubMed: 23554981]

113. Seo S, Mullins RF, Dumitrescu AV, Bhattarai S, Gratie D, Wang K, Stone EM, Sheffield V, Drack AV. Subretinal gene therapy of mice with Bardet-Biedl syndrome type 1. Invest Ophthalmol Vis Sci. 2013;54(9):6118–32. doi:10.1167/iovs.13-11673. [PubMed: 23900607]

114. Breuel S, Vorm M, Brauer AU, Owczarek-Lipska M, Neidhardt J. Combining Engineered U1 snRNA and Antisense Oligonucleotides to Improve the Treatment of a BBS1 Splice Site Mutation. Mol Ther Nucleic Acids. 2019;18:123–30. doi:10.1016/j.omtn.2019.08.014. [PubMed: 31541798]

115. Drack AV, Bhattarai S, Thomas J, Stalter E, Datta P, Hsu y, Garrison J, Searby C, Vandenberghe LH, Heon E, et al. ; Retinal degeneration in BBS10 mice is ameliorated by subretinal gene replacement. Invest. Ophthalmol. Vis. Sci. 2020;61(7):1914..

116. Hanke-Gogokhia C, Chiodo VA, Hauswirth WW, Frederick JM, Baehr W. Rescue of cone function in cone-only Nphp5 knockout mouse model with Leber congenital amaurosis phenotype. Mol Vis. 2018;24:834–46. [PubMed: 30713422]

117. Barbelanne M, Hossain D, Chan DP, Peranen J, Tsang WY. Nephrocystin proteins NPHP5 and Cep290 regulate BBSome integrity, ciliary trafficking and cargo delivery. Hum Mol Genet. 2015;24:2185–200. doi:10.1093/hmg/ddu738. [PubMed: 25552655]

Author Manuscript Author Manuscript Author Manuscript Author Manuscript

118. Boye SE, Huang WC, Roman AJ, Sumaroka A, Boye SL, Ryals RC, Olivares MB, Ruan Q, Tucker BA, Stone EM, et al. Natural history of cone disease in the murine model of Leber congenital amaurosis due to CEP290 mutation: determining the timing and expectation of therapy. PLoS One. 2014;9:e92928. [PubMed: 24671090]

119. Cideciyan AV, Aleman TS, Jacobson SG, Khanna H, Sumaroka A, Aguirre GK, Schwartz SB, Windsor EAM, He S, Chang B, et al. Centrosomal-ciliary gene CEP290/NPHP6 mutations result in blindness with unexpected sparing of photoreceptors and visual brain: implications for therapy of Leber congenital amaurosis. Hum Mutat. 2007;28:1074–83. [PubMed: 17554762]

120. Cideciyan AV, Jacobson SG, Drack AV, Ho AC, Charng J, Garafalo AV, Roman AJ, Sumaroka A, Han IC, Hochstedler MD, et al. Effect of an intravitreal antisense oligonucleotide on vision in Leber congenital amaurosis due to a photoreceptor cilium defect. Nat Med. 2019;25:225–28. [PubMed: 30559420]

121. Sumaroka A, Garafalo AV, Semenov EP, Sheplock R, Krishnan AK, Roman AJ, Jacobson SG, Cideciyan AV. Treatment potential for macular cone vision in leber congenital amaurosis due to CEP290 or NPHP5 mutations: predictions from artificial intelligence. Invest Ophthalmol Vis Sci. 2019;60:2551–62. [PubMed: 31212307]

122. Gardiner KL, Cideciyan AV, Swider M, Dufour VL, Sumaroka A, Komáromy AM, Hauswirth WW, Iwabe S, Jacobson SG, Beltran WA, et al. Long-term structural outcomes of late-stage rpe65 gene therapy. Mol Ther. 2020;28:266–78. [PubMed: 31604676]

123. Maguire AM, Bennett J, Aleman EM, Leroy BP, Aleman TS. Clinical perspective: treating RPE65-associated retinal dystrophy. Mol Ther. 2020;29:442–63. doi:10.1016/j.ymthe.2020.1011.1029. Online ahead of print. [PubMed: 33278565]

Author Manuscript Author Manuscript Author Manuscript Author Manuscript

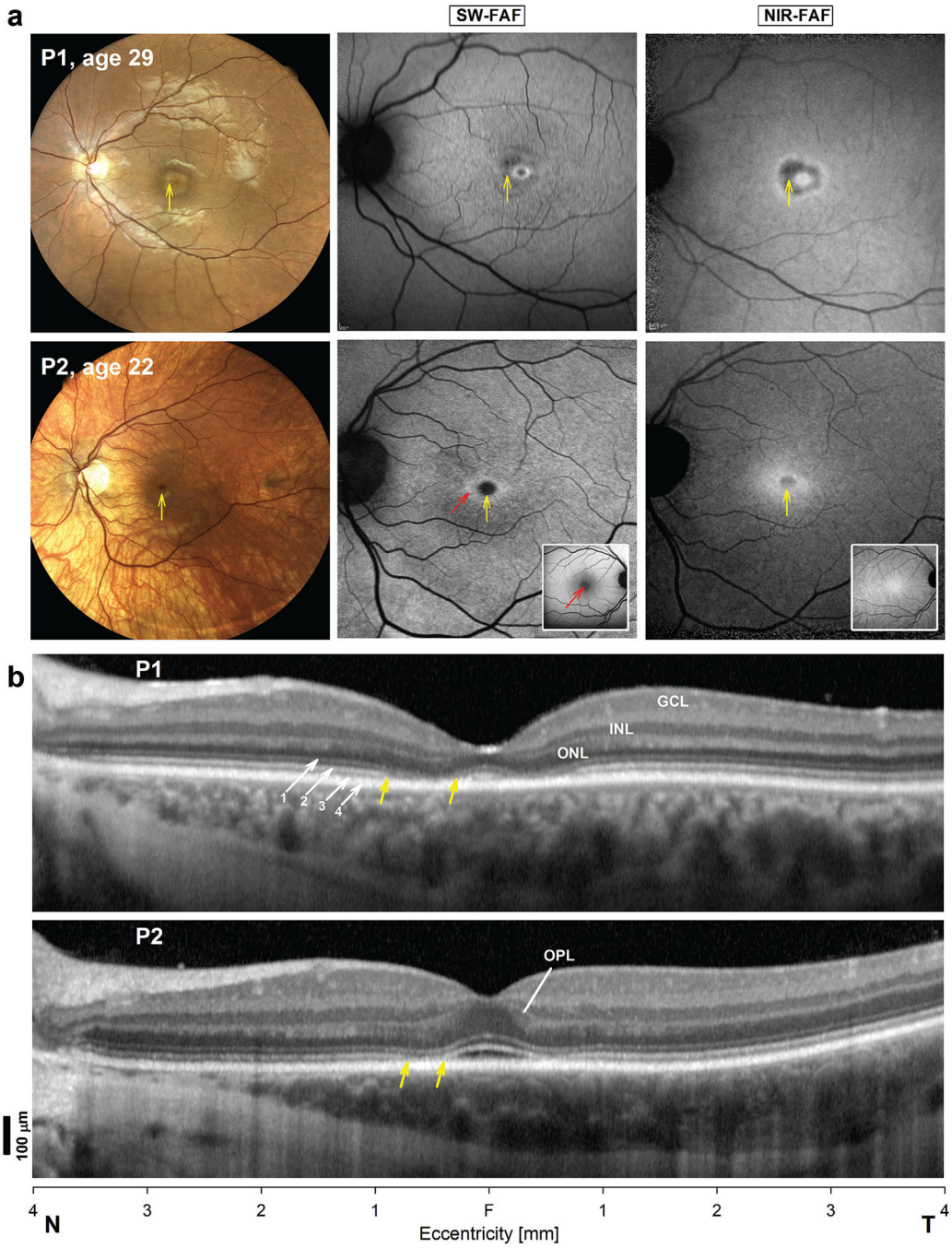

Figure 1.

En-face multimodal imaging in BBS7 patients. (a) Wide angle color fundus photography and fundus autofluorescence elicited with short-wavelength (SW-FAF) and near-infrared (NIR-FAF) excitation lights in both patients. The images correspond to an intermediate visit on their follow up (P1, age 29; P2, age 22) with the highest quality, wide-angle color fundus photography available. Normal appearance of SW-FAF and NIR-FAF imaging are shown as insets of P2. Vertical yellow arrows point to depigmented halo around the foveal center in P1 and to a darker than the surrounding center in P2. Diagonal red arrow on the SW-FAF

Author Manuscript Author Manuscript Author Manuscript Author Manuscript

image of P2 points to juxtafoveal region of increased SW-FAF, which is close to the normal ring of increased autofluorescence caused in the normal subject by a local reduction of the macular pigment optical density in the juxtafovea (shoulder of the macular pigment) in a large proportion of otherwise normal subjects. Representative normal FAF images are shown as insets forcomparison. (b) SD-OCT horizontal, 8 mm cross sections through the fovea of the patients. Nuclear layers are labeled in P1: outer nuclear layer = ONL, inner nuclear layer = INL, ganglion cell layer = GCL. Outer retinal sublaminae are labelled (*diagonal arrows*) according to conventional nomenclature: 1. Outer limiting membrane (OLM), 2. Inner segment ellipsoid region (ISe or EZ), 3. The contact cylinder between the apical RPE microvilli and the photoreceptor outer segments tips, or interdigitation zone (IZ), 4. Basal RPE and Bruch's membrane (RPE/BrM). The outer plexiform layer (OPL) is also labelled in P2. Vertical yellow arrows in the patients denote juxtafoveal segment with abrupt outer retinal (OLM, EZ and IZ) changes where the retina transitions from a near normal appearance on SW- and SW-FAF imaging to deep hypoautofluorescence in (a). Scale bars to the left. T, temporal, N, nasal retina.

Author Manuscript Author Manuscript Author Manuscript Author Manuscript

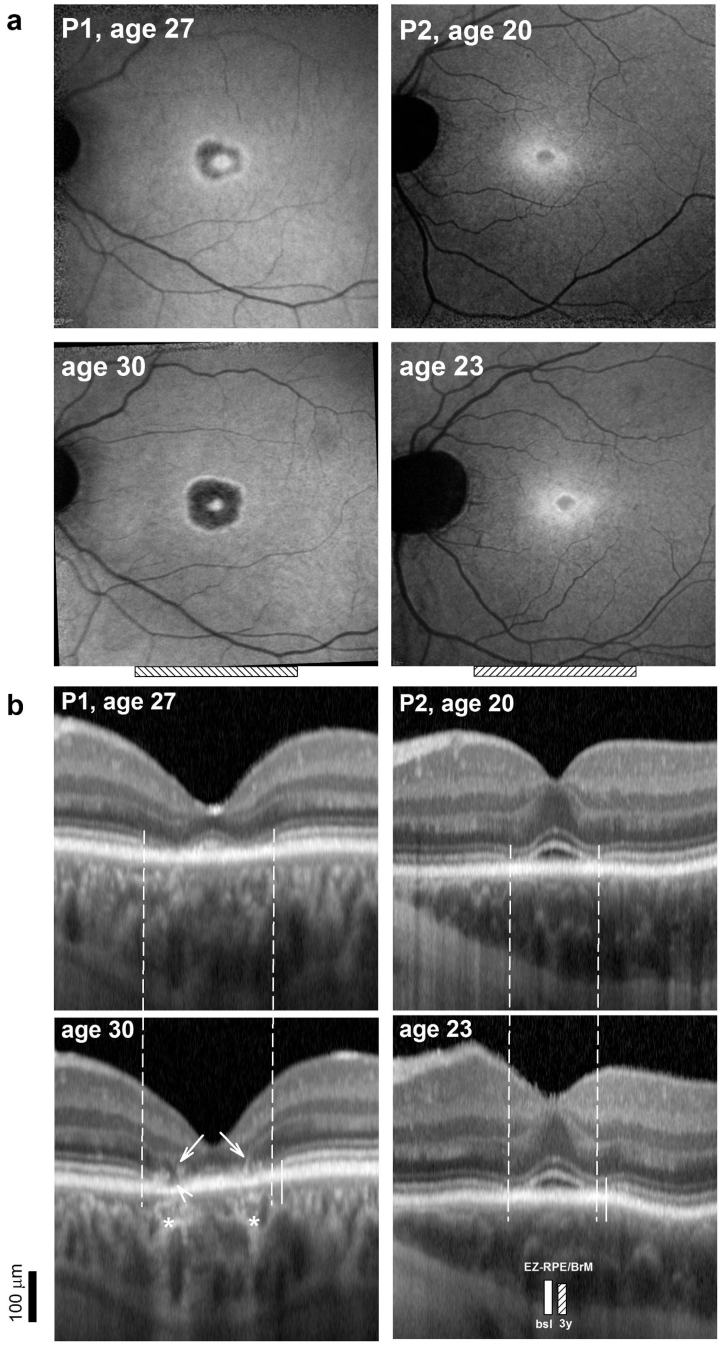

Figure 2.

Longitudinal changes in retinal structure over a three-year interval in BBS7. (a) NIR-FAF images in both patients at two visits. (b) Magnified 2 mm-long SD-OCT cross-sections from the two visits. Horizontal dashed bar at the bottom of NIR-FAF panels in (a) delimit the horizontal extent sampled by the OCT scans. Vertical dashed lines define the peripheral boundary of the juxtafoveal area hypoautofluorescence on NIR-FAF at the first visit that corresponds with a juxtafoveal segment where the EZ band is interrupted. Vertical short solid line parallel to the dashed lines in temporal retina denotes the location of the re-

Author Manuscript Author Manuscript Author Manuscript Author Manuscript

emergence of the EZ band at 3 years which corresponds with the centrifugal movement of this transitional zone. Asterisks = juxtafoveal increased posterior signal scattering due to RPE depigmentation. Arrows point to linear intraretinal hyperreflectivities that may reflect both intraretinal pigment migration and/or Muller cell hypertrophy. Arrowhead points to an hyporreflective area apical to the basal RPE/BrM that appears on follow up in P1. Vertical bars in P2 compared the length of the distance between the EZ and the RPE/BrM at baseline compared to 3 years of follow up.

Author Manuscript Author Manuscript Author Manuscript Author Manuscript

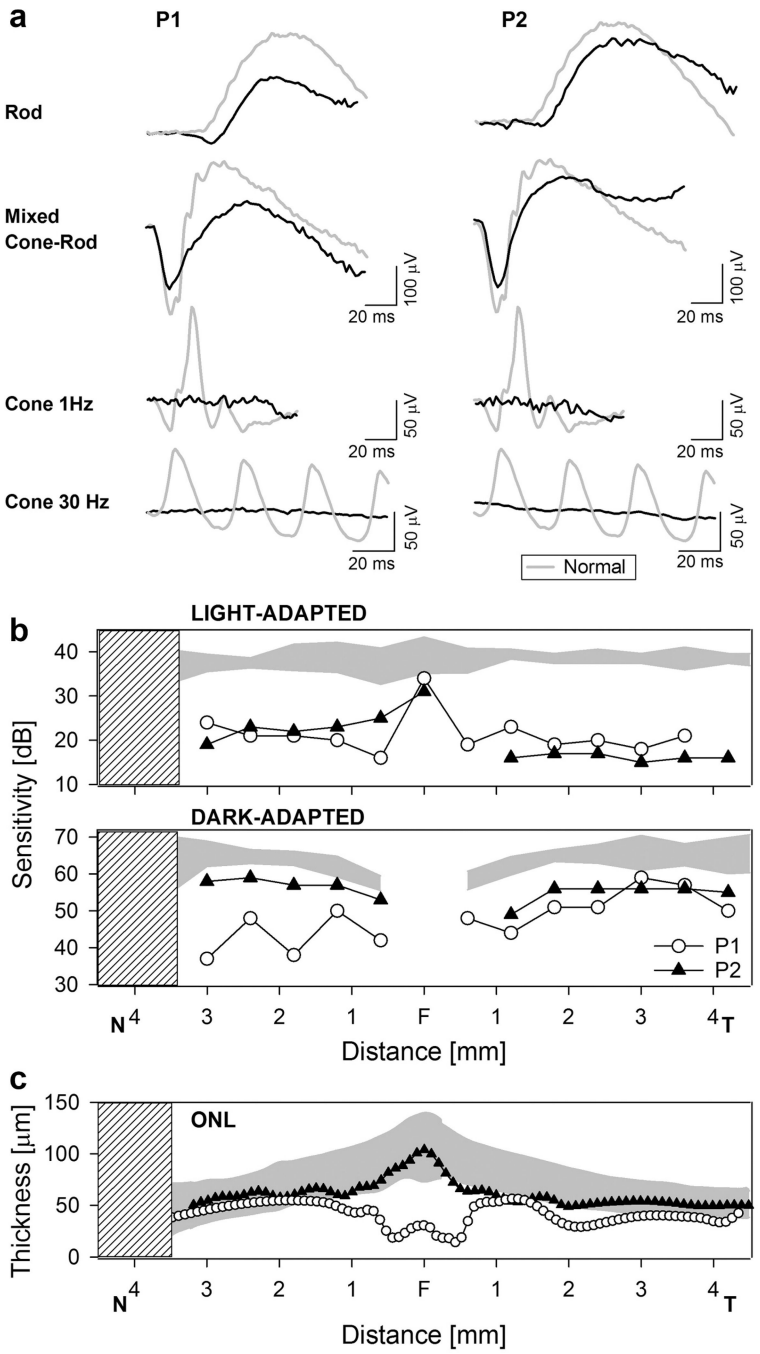

Figure 3.

(a) Standard full-field ERGs in the patients compared with a representative normal subject (gray traces). (b) Light-adapted achromatic and dark-adapted chromatic (500 nm) horizontal sensitivity profiles in the patients compared with the normal range (gray bands, normal mean ± 2SD). Sensitivities to the 500-nm stimulus are confirmed mediated by rods through the use of spectral sensitivity (500 nm – 650 nm) differences. Hatched bar denotes the location of the blind spot. N, nasal. T, Temporal. (c) Thickness of the outer nuclear layer (ONL) along

Author Manuscript Author Manuscript Author Manuscript Author Manuscript

the horizontal meridian at eccentricities that co-localize with the sensitivities measured with static perimetry in (B). Gray bands: normal limits (mean ± 2SD).

Author Manuscript Author Manuscript Author Manuscript Author Manuscript

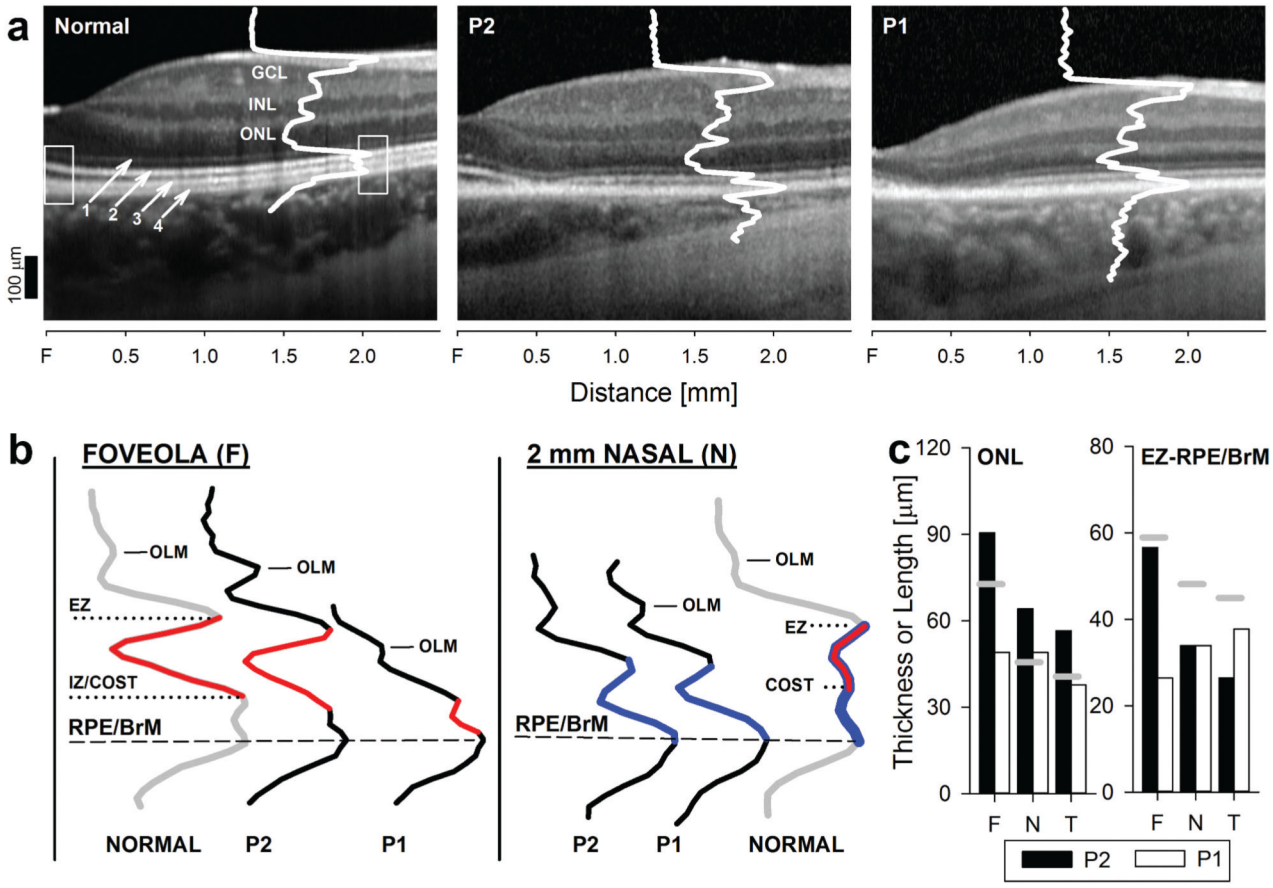

Figure 4.

(a) Magnified 2.5 mm horizontal SD-OCT cross-sections from the fovea into the nasal retina in the two patients on their first visit are compared with a representative normal subject. Overlaid white traces are LRPs from a location ~2 mm nasal from the foveola. (b) LRPs segments distal to the outer limiting membrane (OLM) are magnified to explore changes in the outer retinal sublaminae. LRPs from the foveola and 2 mm nasal [white boxes overlaid on OCT scans in (A)] are compared with normal LRPs (gray traces). The various peaks that correspond with the different outer retinal sublaminae are labelled as in Figure 1. At the foveola, LRP segments colored red denote the signal between the ellipsoid region of photoreceptor inner segments (ISe or EZ) and the contact cylinder between the apical RPE microvilli and the cone outer segment tips (COST), which relates to the length of the foveolar cone outer segment length. LRP segments in blue at the 2 mm location denote the signal that bridges the distance between the ISe and the apical RPE/BRM, which relates to the distance spanned by rod, and intermingled cone (overlapping red segment) outer segments. (c) Thickness of the ONL and the length of the ISe-to-RPE/BrM in patients compared to the lower limit of normal (mean – 2SD) for both parameters (gray horizontal bars). F, foveola. N and T are measures from 2 mm nasal and 3.6 mm temporal to the fovea, respectively.

Author Manuscript Author Manuscript Author Manuscript Author Manuscript

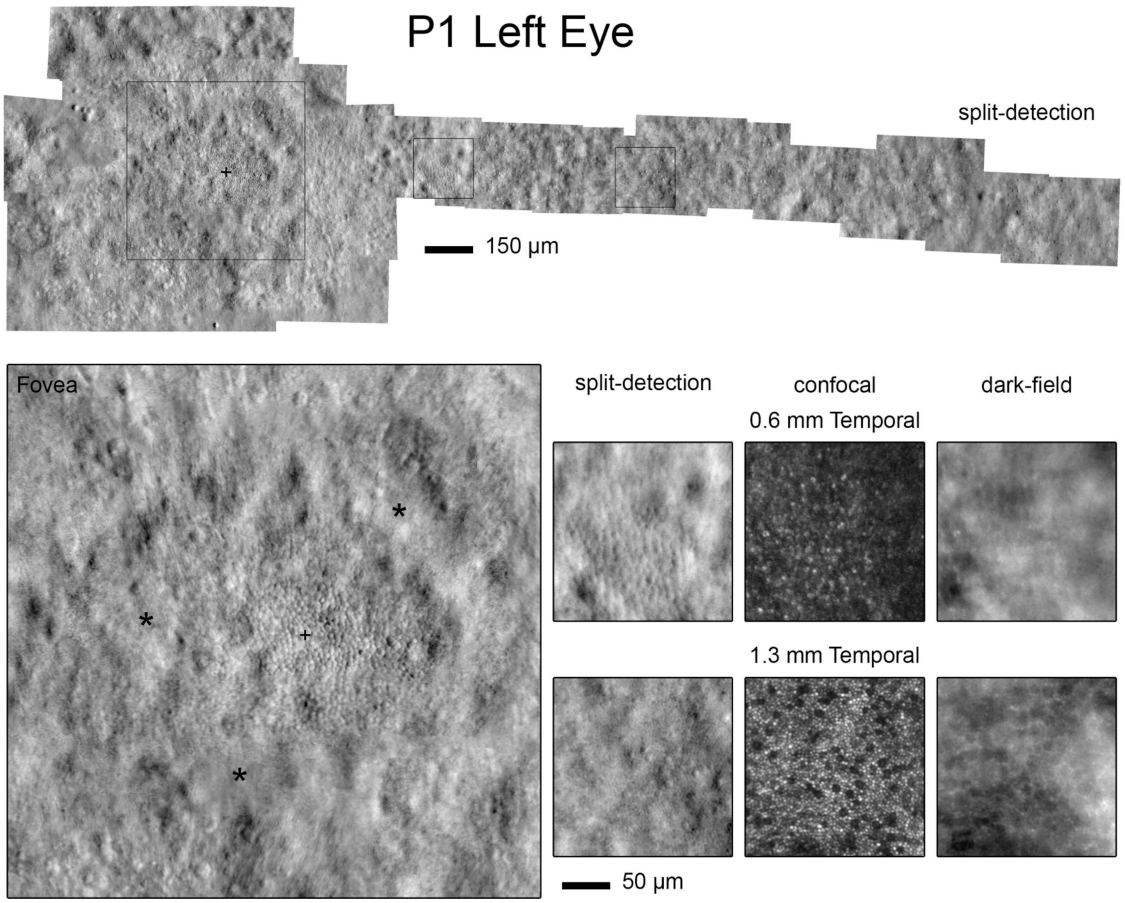

Figure 5.

Adaptive optics images in P1. **Top**. Split-detection adaptive optics montage of the inner segment mosaic. Widespread loss of cone inner segments is observed. **Bottom**. Magnified regions of interest. Split-detection adaptive optics imaging at the fovea (large image) reveals an intact mosaic, cross-hair located at the reduced peak cone density of 31,736 cones/mm^2. Asteriskscorrespond to the bull's eye lesion where the cone mosaic is no longer visible. Split-detection, confocal and dark-field adaptive optics images at 0.6 mm Temporal () show a pocket of retained cone inner and waveguiding outer segments and retinal pigment epithelium, respectively. At 1.3 mm Temporal (eccentricity of) cone and rod densities are reduced, cones do not normally waveguide while rods do and retinal pigment epithelial cell density is normal.

Author Manuscript Author Manuscript Author Manuscript Author Manuscript

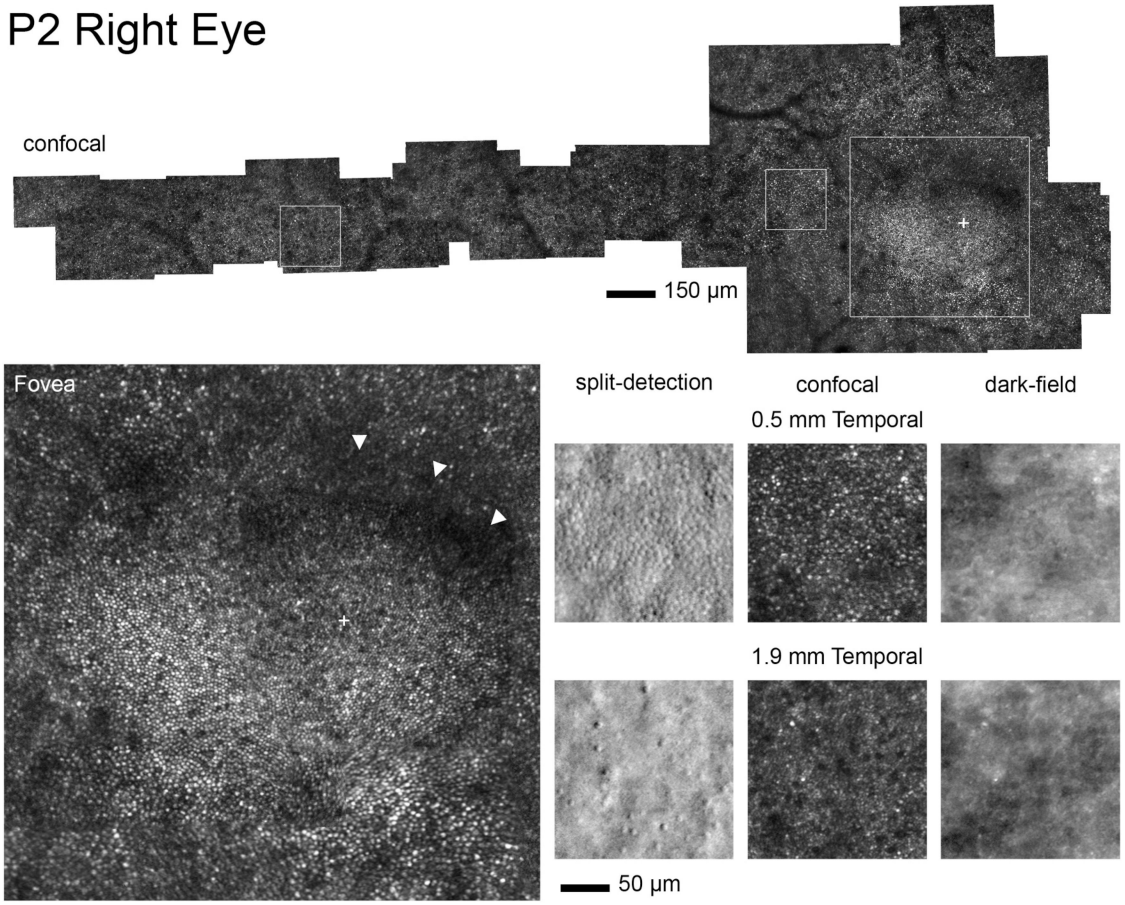

Figure 6.

Adaptive optics images in P2. **Top**. Confocal adaptive optics montage of the photoreceptor mosaic. Widespread loss of cone waveguiding is observed albeit with abnormally retained waveguiding in the temporal parafovea and normal-appearing waveguiding in the foveal center. **Bottom**. Magnified regions of interest. Confocal adaptive optics imaging at the fovea (large) reveals an intact and waveguiding mosaic, cross-hair located at the reduced peak cone density of 97,814 cones/mm^2. Arrowheads identify a region of dimly waveguiding cones, perhaps a precursor to a bull's eye lesion. Split-detection and confocal adaptive optics images at 0.5 mm Temporal again show the cone inner segment mosaic with mottled but retained waveguiding. At 1.9 mm Temporal cone and rod densities are reduced and cones do not normally waveguide while the rods do. Dark-field images show the RPE mosaic.